



Influence of magma-poor versus magma-rich passive margins on subduction initiation

A. Auzemery^{a,b,*}, P. Yamato^{b,c}, T. Duretz^{b,d}, E. Willingshofer^a, L. Matenco^a, K. Porkoláb^{a,e}

^a Utrecht University, Faculty of Geosciences, Department of Earth Sciences, Netherlands

^b Université de Rennes, CNRS, Géosciences Rennes - UMR 6118, F-35000 Rennes, France

^c Institut Universitaire de France (IUF), France

^d Institut für Geowissenschaften, Goethe-Universität Frankfurt, Frankfurt am Main, Germany

^e Institute of Earth Physics and Space Science, Sopron, Hungary

ARTICLE INFO

Article history:

Received 13 April 2021

Revised 27 October 2021

Accepted 25 November 2021

Available online 29 November 2021

Handling Editor: T. Gerya

Keywords:

Subduction initiation

Passive margins rheological coupling

Magma-rich and magma-poor passive margins

Alps

Hellenides/Dinarides

ABSTRACT

We present a new numerical modelling study of subduction initiation at (hyper-extended) magma-poor and magma-rich continental passive margins. In particular, we test how the structure and rheological stratification of these two end-member types control the formation and thermo-mechanical evolution of subduction zones. The serpentinization of mantle lithosphere in a magma-poor continental rifted margin leads to rheological decoupling at the base of the continental crust, which induces shear localization during subsequent shortening. Under these conditions, a shear zone propagates into the mantle lithosphere and leads to subduction initiation at the transition between ocean and passive margin. In contrast, a magma-rich rifted continental margin is rheologically coupled, which creates a buttressing effect and transfer of deformation into the oceanic domain during shortening, where the subduction zone initiates. These results are quantitatively compared and in agreement with the geological record of subduction initiation in the Alps and Dinarides – Hellenides, where the relics of end-member types of continental rifted margins of the same Adriatic micro-continent bordering the Alpine Tethys and Neotethys oceans, respectively, are observed.

© 2021 The Authors. Published by Elsevier B.V. on behalf of International Association for Gondwana Research. This is an open access article under the CC BY license (<http://creativecommons.org/licenses/by/4.0/>).

1. Introduction

Recent studies have shown that the mechanics of subduction initiation remains a critical plate tectonic process that is still poorly understood (Hall, 2019; Stern & Gerya, 2018). These studies emphasize that pre-existing tectonic plates configurations and density contrasts across mechanically weak zones are key ingredients for subduction initiation (e.g. Arcay et al., 2020; Nikolaeva et al., 2010). These conditions can be met at oceanic transform and major fracture zones or in mantle plume settings, where strong lateral density and strength contrasts exist (e.g. Cloetingh et al., 2021; Whattam & Stern, 2015). Ocean-continent transitions also meet these conditions, but direct evidence for subduction initiation at passive margin is scarce (Crameri et al., 2020; Gurnis

et al., 2004). These observations and models have led to the idea that externally driven processes such as subduction zone invasion are needed for the genesis of subduction zones at continental margins (Crameri et al., 2020; Duarte et al., 2013; Zhou et al., 2020). Although this mechanism may explain some natural examples (e.g. western edge of the Pacific plate, Hall, 2019; South Sandwich, van de Lagemaat et al., 2021), its spontaneous retreating mode of subduction (Zhou et al., 2020) contrasts with the geological record of subduction initiation at magma-poor continental margins such as in the Pyrenees or the European Alps orogenic systems (McCarthy et al., 2018), suggesting that subduction initiation must have occurred at passive margins during the plate tectonics history.

Subduction initiation at passive margin requires driving forces to exceed the strength of the ocean-continent transition (Baes & Sobolev, 2017; Cloetingh et al., 1989; Faccenna et al., 1999; Nikolaeva et al., 2010), which is subject to transient changes during thermal relaxation (e.g. Zhong & Li, 2019). Together with the rheological stratification of the passive margin lithosphere (Faccenna

Abbreviations: MPPM, (Magma Poor Passive Margin); MRPM, (Magma Rich Passive Margin); OCT, (Ocean-Continent Transition).

* Corresponding author at: Utrecht University, Earth Simulation Lab, Princeton-laan 3584 CB Utrecht, Netherlands.

E-mail address: a.auzemery@uu.nl (A. Auzemery).

et al., 1999; Goren et al., 2008), these parameters are inferred to be critical for the locus of subduction initiation (Auzemery et al., 2021a; Nikolaeva et al., 2011). These modelling studies have shown that, under compressive stress regime, deformation is focussed in the ductile lower continental crust when the oceanic lithosphere at the margin is older than ~50 Myr and the continental lithosphere is relatively thin (~100–150 km). When such conditions are met, subduction initiation is physically feasible by the evolution of major shear zones in the ductile crust that propagates into the mantle where thermal softening facilitates the formation of a subduction zone (Auzemery et al., 2020; Kiss et al., 2020). In contrast, deformation localises within the rheologically weaker oceanic lithosphere, when they are younger than 50 Myr and/or in case of high convergence rate ($>2 \text{ cm.yr}^{-1}$, Zhong & Li, 2019), leading to intra-oceanic subduction.

All previous modelling studies have not yet quantified the impact of significant differences in geometry and rheology between magma-rich and magma poor continental passive margins (MRPM and MPPM, respectively) for subduction initiation (Fig. 1), constrained by the available observational record (Geoffroy, 2005; Sengör & Burke, 1978; Tugend et al., 2020; White et al., 1987). In particular, MRPM are typically driven by mantle upwelling and are associated with significant magmatic activity during rifting (Fig. 1a, Corti, 2009; Li et al., 2020; White et al., 1987). Important is the presence of magmatic intrusions and extrusions as well as underplating of mafic bodies at the base of the crust, which significantly increases its effective strength after cooling (Kelemen & Holbrook, 1995; Paton et al., 2017). In contrast, MPPM are typically driven by lithospheric stretching without significant decompressional melting magmatism, resulting in exhumation and hydration of the mantle in the footwall of major detachments (Fig. 1b, Brun & Beslier, 1996; Clerc et al., 2018; Manatschal et al., 2001; Mohn et al., 2012). The hydration-induced serpentinization penetrates into the mantle lithosphere and creates rheologically weak decollement layers that are prone to tectonic reactivation (Guillot et al., 2015; Hilairet et al., 2007).

In this study, we aim to understand and quantify subduction initiation in the vicinity of contrasting end-member types of passive continental margins (MRPM and MPPM) during far-field induced shortening by means of thermo-mechanical numerical modelling, constrained by the available observational record. In particular, we test the influence of differences in crustal and lithospheric structure, composition and evolution of deformation. A two-steps strategy is adopted to understand both first order controlling mechanisms and the more detailed response. In a first step,

we assess the deformational response to the degree of rheological crust-mantle coupling at an idealised continental passive margins. In a second step, we use realistic geometries and compositions of magma-poor and magma-rich continental passive margins to test their specific impact on subduction initiation. The modelling results are validated against observations and quantitative reconstructions of the Adriatic micro-continent, an ideal well-studied area that contains the record of both end-member types of passive continental margins (MRPM and MPPM). This record is exposed in two European orogenic systems, the Dinarides-Hellenides and the Alps, for the MRPM and the MPPM, respectively.

2. Modelling approach

2.1. Methods

We performed two-dimensional (2D) thermo-mechanical modelling to simulate the shortening of a visco-elastic-plastic lithosphere. The finite-difference, marker-in-cell code (MDoodz; Duretz et al., 2016) solves the equations of momentum (1) and mass conservation (2), as well as the heat equation (3) formulated as:

$$\frac{\partial \tau_{ij}}{\partial x_j} - \frac{\partial P}{\partial x_i} = -\rho g_i \quad (1)$$

$$\frac{\partial v_i}{\partial x_i} = 0 \quad (2)$$

$$\rho C_p \frac{DT}{Dt} = \frac{\partial}{\partial x_i} \left(k \frac{\partial T}{\partial x_i} \right) + Q_r + Q_{SH} \quad (3)$$

where v is the velocity vector, T is the temperature, k is the thermal conductivity, ρ is the density, C_p is the heat capacity, Q_r is the radiogenic heat production, τ is the deviatoric stress tensor, $\dot{\epsilon}$ is the deviatoric strain rate tensor, P is the pressure and g is the gravity acceleration vector. The term $Q_{SH} = \tau_{ij} \dot{\epsilon}_{ij}^{vp}$ describes the production of heat by visco-plastic (vp) dissipation (shear heating). For details regarding the mathematical model and algorithms, see supplementary material S1.

The model domain is a section of $3000 \times 500 \text{ km}$ and the grid resolution is $1 \times 1 \text{ km}$ in both dimensions (Fig. 2). The model top boundary is a true free surface (Duretz et al., 2016), computed as:

$$\frac{Dh}{Dt} = \frac{\partial}{\partial x_i} \left(D \frac{\partial h}{\partial x_i} \right) + \dot{s} \quad (4)$$

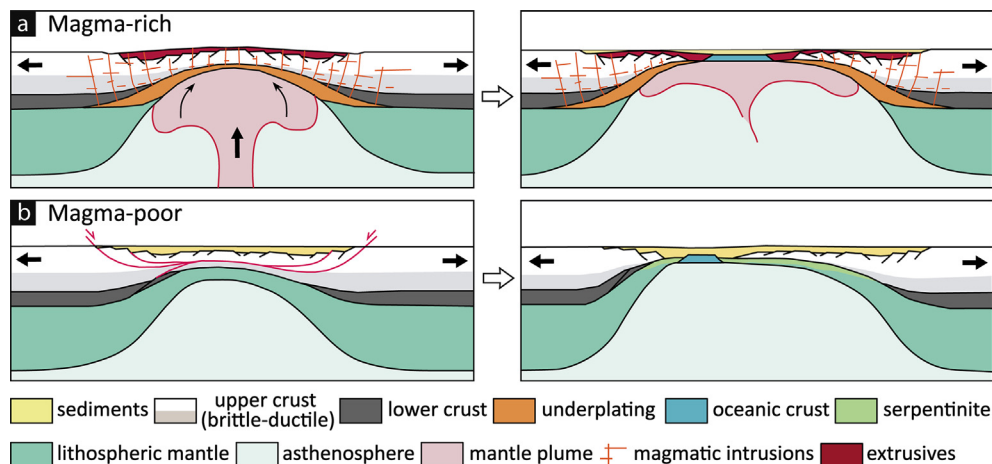


Fig. 1. Cartoons showing first order characteristics of a) magma-rich (inspired from Geoffroy, 2005); and b) magma-poor continental rifted margins (inspired from Mohn et al., 2012) for two evolutionary stages.

Table 2

Rheological and thermal parameters used for the magma-poor and magma-rich passive margins models.

	h O/C (km)	ρ (kg.m ⁻³)	k (W.m ⁻¹ .K ⁻¹)	Qr (W.m ⁻³)	Φ (°)	A (Pa ⁻ⁿ .s ⁻¹)	v (m ³ .mol ⁻¹)	f	n	G (Pa)	Q (J.mol ⁻¹)	Ref.
Sediments	2 / 0											
sediment1 (calcite)		2600	2.5	2.0e-6	20	1.59e-25	0	0	4.7	1.0e10	297.0e3	K_90
sediment2 (mica)		2400	2.5	2.0e-6	20	1.00e-138	0	0	18.0	1.0e10	51.0e3	K_90
Continental crust MPPM	36											
Upper (dry quartzite)	24	2800	2.7	9.0e-7	30	3.98e-19	0	0	2.4	3.5e10	156.0e3	R_95
Lower (felsic granulite)	12	2800	2.7	4.0e-7	30	2.01e-21	0	0	3.1	3.5e10	243.0e3	R_95
Hydrated mantle (serpentinite)		2800	2.7	9.0e-7	30	8.83e-22	0	0	4.2	3.5e10	445.0e3	H_07
Continental crust MRPM	36											
Upper (dry quartz)	20	2800	2.7	9.0e-7	30	3.98e-19	0	0	2.4	3.5e10	156.0e3	R_95
Lower (felsic granulite)	16	2800	2.7	4.0e-7	30	2.01e-21	0	0	3.1	3.5e10	243.0e3	R_95
Extrusive (wet olivine)		2900	3.2	1.0e-10	30	1.10e-16	11.0e-6	0	3.5	3.5e10	530.0e3	H&K_03
Underplating (dry diabase)		3000	2.7	9.0e-7	30	5.04e-28	0	0	4.7	3.5e10	485.0e3	M_98
Oceanic crust (wet olivine)	8	2900	3	1.0e-7	30	5.68e-27	11.0 e-6	1	3.5	3.5e10	480.0e3	H&K_03
Mantle lithosphere (dry olivine)	96 / 139											
Dislocation creep		3300	3.2	1.0e-10	30	1.10e-16	11.0e-6	0	3.5	3.5e10	530.0e3	H&K_03
Diffusion creep		3300	3.2	1.0e-10	30	1.50e-15	1.5e-16	0	1.0	3.5e10	375.0e3	H&K_03
Asthenosphere (dry olivine)	404 / 361											
Dislocation creep		3300	3.2	1.0e-10	30	1.10e-16	11.0e-6	0	3.5	3.5e10	530.0e3	H&K_03
Diffusion creep		3300	3.2	1.0e-10	30	1.50e-15	1.5e-16	0	1.0	3.5e10	375.0e3	H&K_03

constant asthenosphere temperature of 1330 °C. The resulting temperature at the continental Moho is ~460 °C. When displaying modelling results, we focus on the mechanically significant part of the lithosphere defined by the 1000 °C geotherm (~base of the strength envelope, [Burov, 2011](#)).

In this first step, we carried out 32 numerical models and systematically varied the length and the crustal composition of the passive margin lithosphere, thereby reducing the mechanical coupling between the crust and the mantle lithosphere at the margin. The reference models test 8 different lengths of passive margins changing from 50 km to 400 km, covering most of natural passive margin lengths ([Reston & Manatschal, 2011](#)), as well as 4 different rheologies for the whole crust ([Table 1](#)). The modelling results are used for constructing domain diagrams ([Fig. 3a, b](#)), which allow for mapping the mode of deformation against the length and the crust-mantle coupling of the margin. They thus provide an overview of suitable parameter combinations for subduction initiation and provide a geometric and rheological frame for models with

specificities tailored to represent magma poor and magma rich passive margins.

The second set of models includes the specific crustal characteristics of MPPM and MRPM as illustrated in [Fig. 1](#), with the same thermal base in the oceanic and continental domain for both models. A different flow law was attributed to each material, in agreement with the simulated type of oceanic or continental layered lithosphere, magmatic material and overlying sediments, as well as their lateral distribution, to account for a representative simplification of a more realistic natural scenario (see [Fig. 6a, 7a](#)). To be able to highlight the relevance of crust-mantle coupling and to correlate models with our parametric study, the crust and mantle thicknesses were kept similar. However, a 2-layers model is now used for the continental crust consisting of an upper crust of 20 km thickness with dry quartzite rheology and a lower crust between 20 and 36 km depth where deformation is described by a felsic granulite flow law (see parameters in [Table 2](#)).

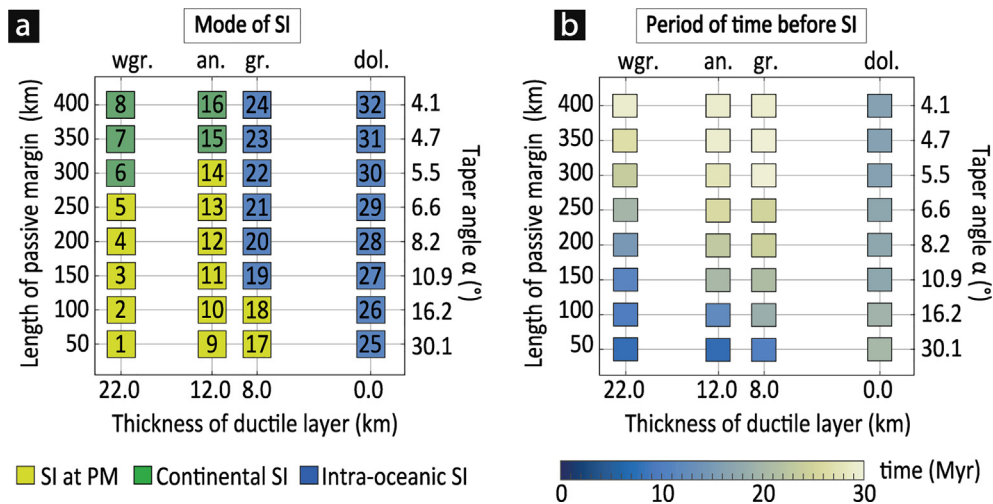


Fig. 3. Results of the parametric study for the reference model: (a) Area diagram showing the influence of continental crust-mantle coupling and length of the lithosphere at passive margin on the mode of subduction initiation. wgr., an., gr., dol., stand for westerly granite, anorthite, granulite, dolerite, respectively. The numbers and colours represent the experiment numbers and the modes of subduction initiation, respectively. The thickness of ductile layer at the onset of deformation is measured between the depth of the stress peak and the base of the continental crust. (b) Time period of subduction initiation measured from t_0 to the incipience of subduction.

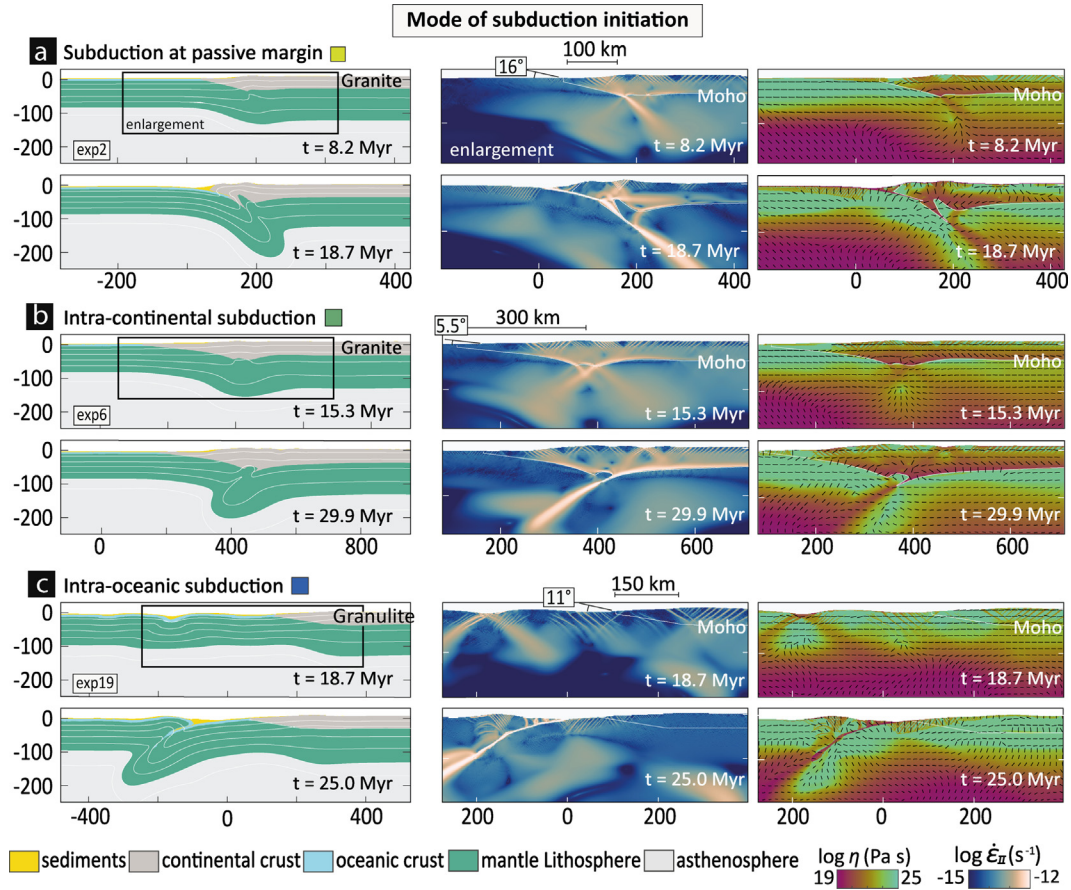


Fig. 4. Mode of subduction initiation observed in the parametric study. (a) Subduction at the passive margin, (b) intra-continental subduction and (c) intra-oceanic subduction. Enlargements display the strain rate and the viscosity at the early stage of underthrusting as well as the direction of the maximum principal stress (σ_1).

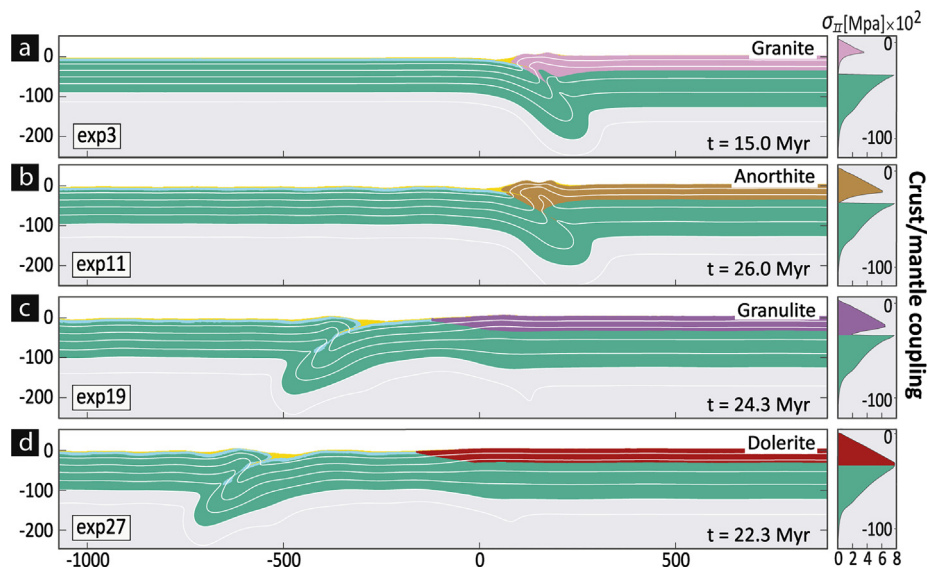


Fig. 5. Left: Role of crust-mantle coupling on the locus of subduction initiation. Crust-mantle coupling is controlled by the composition of the continental crust. Right: Strength profiles where σ_{II} is the second invariant of the deviatoric stress tensor. Length of passive margin is 150 km for all experiments. The different colours in the crust represent the four different compositions of the crust used in this study. Other layers are the same as shown in Fig. 2. Model evolutions are available in the supplementary material S2.

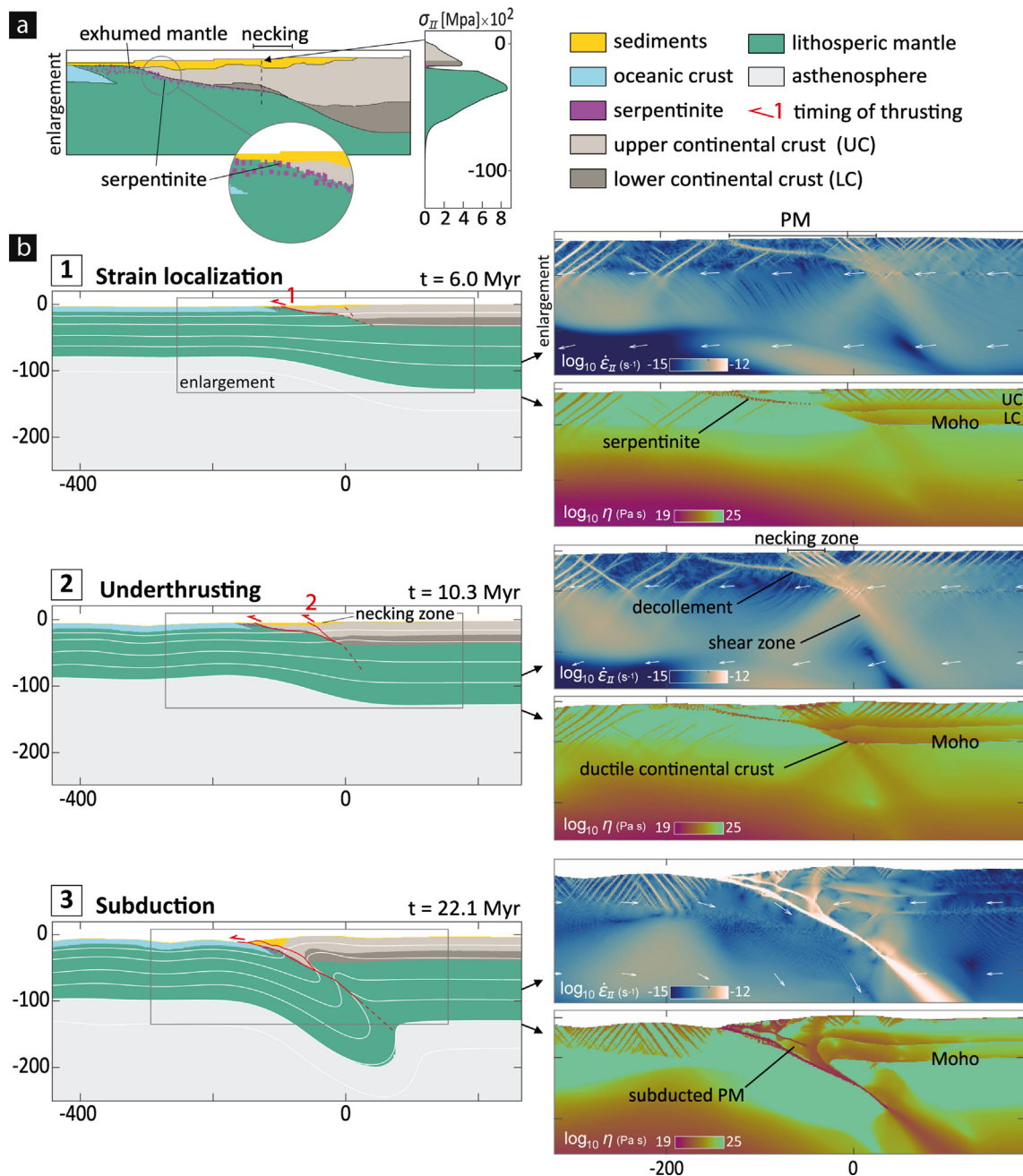


Fig. 6. Subduction initiation for a magma-poor passive margin. Length of passive margin is 150 km. (a) Model setup with an enlargement of the passive margin to show the geometry and the rheological stratification of a magma-poor margin. Strength profile indicates crust-mantle decoupling. (b) Model evolution, illustrating key stages in the subduction initiation process where the left panel shows the deformation of the layers and associated temperature structure. Red numbers indicate the sequence of interpreted shear structures. The right panel shows the distribution of strain rate and viscosity for each time-step. White arrows represent the velocity field. PM is the passive margin. (For interpretation of the references to colour in this figure legend, the reader is referred to the web version of this article.)

2.3. Model limitation

The aim of this study is to provide insights into favourable rheological conditions for subduction initiation at magma rich and magma poor passive continental margin where convergence is orthogonal to the ocean-continent transition. Inherent to the approach are model limitations related to the choice of initial and boundary conditions and the dynamics of the system. Our models do not account for initial 3D variations of crust and lithosphere architecture, structure, and composition, inherited from rifting and passive margin formation. These have recently been implemented and discussed in the modelling studies of [Beaussier](#)

[et al. \(2019\)](#), [Gülcher et al. \(2019\)](#), or [Zhou et al. \(2020\)](#) and are particularly important when convergence is oblique to the inherited structures ([Beaussier et al., 2019](#)) and when subduction initiation takes place by lateral propagation of an existing subduction zone (e.g. [Zhou et al. 2020](#)). Subduction initiation in our study is driven by horizontal forcing imposed by convergent kinematic boundary conditions. Therefore, we do not account for mantle upwelling ([Gerya et al., 2015](#); [Koptev et al., 2019](#); [Koptev et al., 2021](#)) or mantle suction flow ([Baes & Sobolev, 2017](#); [Yamato et al., 2013](#)). Furthermore, we do not account for climate driven variability of sediment supply to the trench controlling the lubrication of the evolving subduction zone ([Sobolev & Brown, 2019](#)). Despite these

simplifications, our 2D models provide a significantly advanced approach to accurately describe the system behaviour and obtain novel insights in the key parameters controlling the mechanism associated with subduction initiation.

3. Modelling results

3.1. Reference model

Using numerical experiments, we have systematically investigated the role of the passive margin length and the degree of crust-mantle coupling on subduction initiation (Table 3 and Fig. 3a). For each rheological configuration presented above, the length of the margin (the wedge in the models) has been varied yielding three end-modes of subduction initiation: subduction at the passive margin, intra-continental subduction and intra-oceanic subduction (Fig. 4a, b, c, respectively). More specifically, intra-continental subduction refers to the subduction of the continental lithospheric mantle under the oceanic lithosphere.

3.1.1. Role of crust-mantle coupling

For a constant length of the passive margin (e.g., 150 km, Fig. 5), variation of continental crust rheology impacts on the degree of crust-mantle coupling and consequently controls the locus of subduction initiation. For instance, the presence of a granitic continental crust allows the decoupling of the crust from the mantle and favours subduction initiation at the margin. In this case, deformation starts at the base of the ductile crust at the ocean-continent transition, where a shear zone develops, which eventually propagates into the mantle lithosphere (Fig. 5a). In contrast, shortening of a strong doleritic or granulitic continental crust, which results in strong crust-mantle coupling, consistently leads to folding of the lithosphere followed by intra-oceanic subduction (Fig. 5c, d).

In this case, early-stage deformation affects the passive margin, which bends downward (Fig. 5c). However, strain does not localize over a long period of time and deformation shifts from the passive margin towards the oceanic domain where subduction occurs.

Models where continental crust is simulated using an anorthite flow law, (intermediate case of coupling) follow a similar evolution as those with a granitic crust. However, subduction at the margin is intricate and folding is observed in the oceanic domain (Fig. 5b). We note that folding is better expressed close to the passive margin than in the middle of the oceanic plate (Fig. 5b, c), likely reflecting stress concentration at the ocean-continent transition. Evidence of this mechanism is highlighted by a decrease of the amplitude and the wavelength of folding from the margin to the ocean (Fig. 5b). In case of stronger coupling (dolerite crust), deformation at the margin is limited and folding mainly affects the oceanic domain (Fig. 5d). Such early intra-oceanic folding leads to higher sedimentation in the newly formed flexural basins (Fig. 5d).

3.1.2. Role of the passive margin length

Our results show that subduction initiation at passive margins requires the development of a shear zone that subsequently propagates into the mantle lithosphere (Fig. 4a). Deformation localizes at the base of the ductile crust of the continental margin, where a shear zone initiates. Varying the passive margin length implies changing the wedge or taper angle (α) of the margin, and thus, the angle at which the ductile lower crust dips towards the continent (Fig. 4a-c). Our results highlight that the likelihood of subduction initiation at passive margins decreases with increasing margin length. For margin lengths in excess of 300 km, equivalent with wedge angles lower than 7°, intra-continental subduction is observed (Figs. 3a and 4b). In contrast, short margin result in initially steeper dip, which favours flow of the ductile crust at the ocean-continent transition and fosters subduction initiation.

Table 3

Overview of model parameters (crustal rheology and passive margin length) and modelling results for the reference models. W. granite is Westerly granite. PM refers to the passive margin.

Id	Continental crust rheology	PM length (km)	Taper angle α (°)	Mode of subduction initiation	Period of time before subduction (Myr)
1	w. granite	50	30.11	Passive margin	7
2	w. granite	100	16.17	Passive margin	9
3	w. granite	150	10.94	Passive margin	11
4	w. granite	200	8.25	Passive margin	15
5	w. granite	250	6.62	Passive margin	19
6	w. granite	300	5.52	Intra-continental	24
7	w. granite	350	4.74	Intra-continental	27
8	w. granite	400	4.15	Intra-continental	29
9	anorthite	50	30.11	Passive margin	6
10	anorthite	100	16.17	Passive margin	13
11	anorthite	150	10.94	Passive margin	21
12	anorthite	200	8.25	Passive margin	23
13	anorthite	250	6.62	Passive margin	26
14	anorthite	300	5.52	Passive margin	27
15	anorthite	350	4.74	Intra-continental	29
16	anorthite	400	4.15	Intra-continental	29
17	granulite	50	30.11	Passive margin	10
18	granulite	100	16.17	Passive margin	19
19	granulite	150	10.94	Intra-oceanic	22
20	granulite	200	8.25	Intra-oceanic	24
21	granulite	250	6.62	Intra-oceanic	26
22	granulite	300	5.52	Intra-oceanic	30
23	granulite	350	4.74	Intra-oceanic	29
24	dolerite	400	4.15	Intra-oceanic	30
25	dolerite	50	30.11	Intra-oceanic	20
26	dolerite	100	16.17	Intra-oceanic	19
27	dolerite	150	10.94	Intra-oceanic	18
28	dolerite	200	8.25	Intra-oceanic	17
29	dolerite	250	6.62	Intra-oceanic	17
30	dolerite	300	5.52	Intra-oceanic	16
31	dolerite	350	4.74	Intra-oceanic	15
32	dolerite	400	4.15	Intra-oceanic	16

A small wedge angle represents a case of a long passive margin where the ductile crust gets gradually thinner towards the ocean-continent transition. When the thickness of the ductile crust gets lower than ca 3.5 km, stresses within this layer get too high and the ductile crust does not act as a decollement anymore. Instead, deformation is transmitted further into the ductile crustal layer toward the continent (Fig. 4b). In this situation, shortening is accommodated by folding of the mantle lithosphere at the margin, resulting in deflection of the continental Moho. In the later stage of the model, strain propagates into the mantle leading to intra-continental subduction (Fig. 4b). The oceanward polarity of the subduction zone is probably controlled by the buttressing effect of the long and overall strong passive margin crust, which is coupled to the mantle lithosphere in the area of the ocean-continent transition. Therefore, our models suggest that the formation of a subduction zone at passive margins is more easily achieved with a steep and decoupled passive margin (Fig. 3a). In other cases, deformation is transmitted toward the continental crust (Fig. 4b) or the oceanic lithosphere (Fig. 4c).

3.1.3. Timing of subduction initiation

Our results highlight an important correlation between geometrical (length of passive margin and margin angle) and rheological (thickness of ductile continental crust) initial conditions with the period of time required for subduction initiation (Fig. 3b). We refer to duration of subduction initiation in our models as the period between the start of shortening (at $t = 0$) and the moment when the continuous shear zone analogous to an incipient subduction plate boundary is established. Furthermore, we use the thickness of the ductile crust as a proxy for the degree of crust-mantle coupling, where a thicker ductile crust represents a decoupled case and vice versa. For a similar convergence rate, initiation of subduction requires less time for a decoupled lithosphere (<10 Myr) than for a coupled lithosphere (>15 Myr, see Fig. 3b), because a weak lower crust favours strain localization early in the evolution of a subduction zone. For the same reason, the length of the margin increases the duration of subduction initiation. An exception exists with strong crust mantle-coupling at the passive continental margin (e.g., crust simulated using dolerite). In such cases subduction initiation does not occur at the passive margin, which deforms over a long period of time, but within the oceanic plate (Fig. 5d). We emphasise that the duration of subduction initiation also includes early phases of distributed deformation of the passive margin prior to strain localization. This phase is longer by ca. 10 Ma for weak margins (e.g., anorthite crust) as opposed to strong margins consisting of doleritic crust as indicated in Fig. 3b.

3.2. Application to magma-poor and magma-rich passive margins

The parametric study allowed us to infer the sensitivity of parameters controlling localization of deformation and subsequent subduction initiation. The next step is to understand the impact of a more realistic 150 km long magma-poor (Fig. 6) and magma-rich (Fig. 7) passive margin geometries and composition for subduction initiation.

3.2.1. Subduction initiation at magma-poor passive margins

The magma-poor passive margin model (Fig. 6a) accounts for the necking of continental crust, resulting in a large omission of the lower crust in distal margin domains and the exhumation and hydration of sub-crustal mantle peridotites at the ocean-continent transition (Brun & Beslier, 1996; Manatschal et al., 2001; Mohn et al., 2012). As in geophysical models, the exhumed mantle shows variable degrees of serpentinization (Bayrakci et al., 2016), which is accounted for in the model by placing distributed patches of serpentinite material within the uppermost

mantle lithosphere, where the mantle is located at the sea floor and below the extended margin (Fig. 6a). The latter represents serpentinization due to normal faulting cutting across the extended margin crust. By implementing these complexities, we account for a relatively weak lithosphere at the ocean-continent transition that represents a thinned continental lithosphere overlying a serpentinized mantle, and therefore, a relatively weak crust-mantle coupling (Fig. 6a).

The evolution of our simulation follows the general trend of a model with crust-mantle decoupling at the base of the margin (Fig. 6b) and includes: the onset of deformation at the ocean-continent transition, the formation of shortening structures across the margin, subsequent propagation of deformation into the mantle lithosphere and finally underthrusting of oceanic lithosphere at the passive margin.

The results show that the thrust-type deformation sequence is younging towards the continent (fault 1 is older than fault 2, Fig. 6b) during the early stage of deformation. Different to the reference models, strain rates are highest ($\sim 10^{-13} \text{ s}^{-1}$) within the serpentinized mantle, (Fig. 6b1) and not within the ductile crust. The model shows that at ca. 10 Ma of shortening, shear along the weak serpentinites links up with shear within the ductile crust below the necking zone to form a throughgoing shear zone at the base of crust (Fig. 6b2). Furthermore, this shear zone is linked to a major thrust-type structure (number 2 in Fig. 6b2) that evolves near the necking zone where the margin is thickening, and the wedge angle increases. Subsequently, the distal margin is thrust below the continental lithosphere and accreted to the overriding plate at depth of 25–35 km (Fig. 6b3). At the position of the former distal margin a thick sedimentary wedge developed ~ 15 Myr after the onset of convergence.

3.2.2. Subduction initiation at magma-rich passive margin

The model involving a magma-rich passive margin accounts for magmatic underplating, as well as mafic intrusions and extrusions, as a result of partial melting of the mantle lithosphere (Geoffroy, 2005). Magmatic underplates are often characterized by high-velocity seismic zones in the lower crust (Kelemen & Holbrook, 1995; Sapin et al., 2021). Mafic intrusions are gabbroic complexes (sills, dikes) distributed across the MRPM. Their equivalents at the surface correspond to large basaltic lava flows identified as seaward dipping reflectors on seismic reflection data (Paton et al., 2017; White et al., 1987). We ascribe a dolerite rheology to the magmatic underplatings while magmatic extrusions are simulated by wet olivine. In the model we implement these features by accounting for a margin that exhibits a continental crust intruded by mafic rocks. The evolution of our model during subduction initiation of a MRPM follows the general trend of a model with a strong crust-mantle coupling at the margin (Fig. 7b). It features first distributed deformation at the ocean-continent transition, migration of deformation and folding of the oceanic lithosphere, followed by intra-oceanic subduction.

The modelling shows that the addition of magmatic lithologies strengthens the passive margin close to the ocean-continent transition and increases the crust-mantle coupling, preventing strain localization. Therefore, most of the strain is localized in the oceanic lithosphere near the ocean-continent transition, while less deformation is observed in the ductile layer of the proximal continental margin (Fig. 7b1). The oceanward underthrusting takes place 350 km away from the margin, at one of the conjugate shear structures (Fig. 7b2). Although the oceanic domain is 1500 km long, strain localizes relatively close to the ocean-continent transition, similarly to the reference model (Fig. 5c). The subsequent development of a subduction zone is associated with the development of an accretionary wedge, which is recognisable ~ 12 Myr after the onset of convergence (Fig. 7b3).

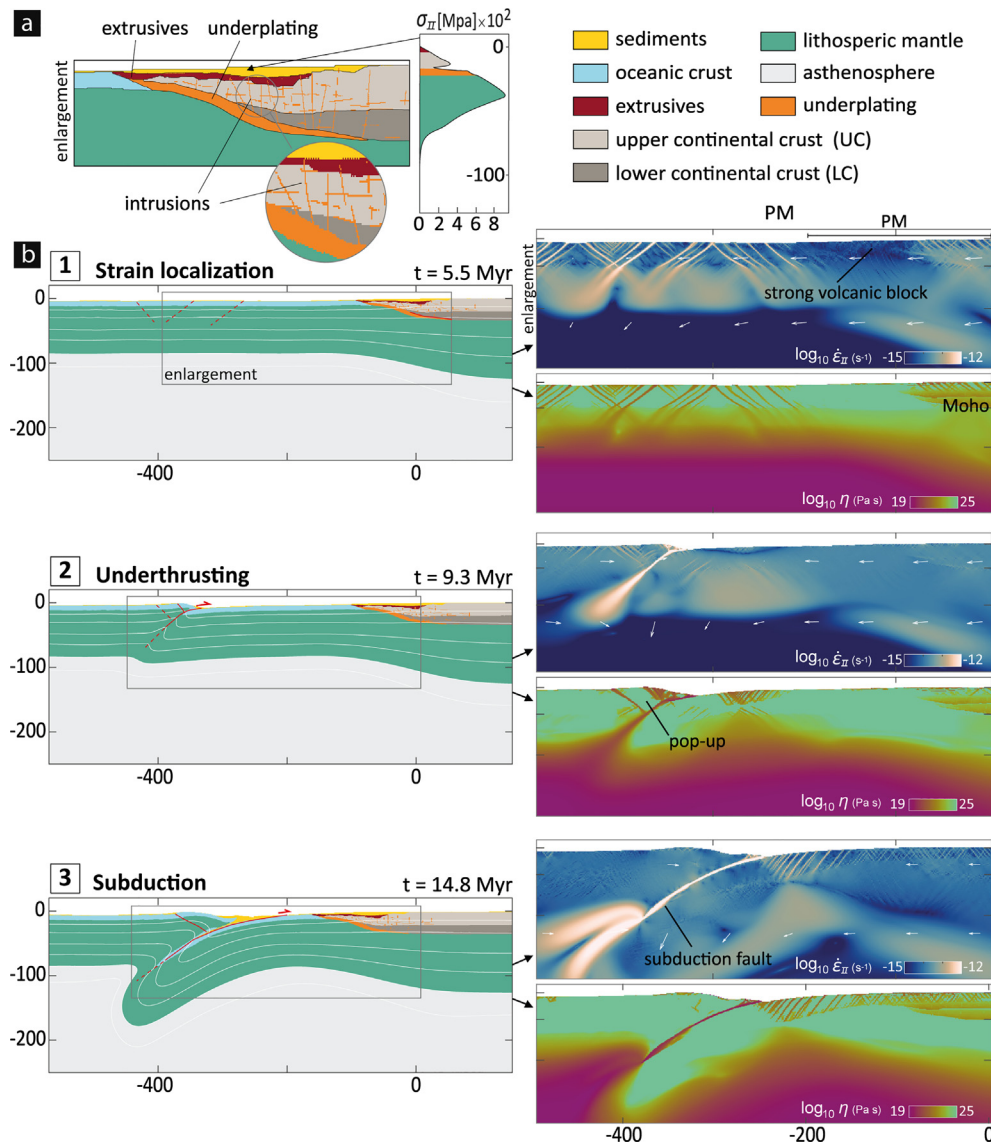


Fig. 7. Subduction initiation for a magma-rich passive margin with a margin length of passive margin is 150 km. (a) Model setup with an enlargement on the passive margin to highlight the geometry and rheological stratification of a magma-rich margin. (b) Model evolution illustrating key stages in the subduction initiation process where the left panel shows the deformation of the layers and associated temperature structure. The right panel shows the distribution of strain rate and viscosity for each time-step. White arrows represent the velocity field. PM is passive margin.

3.2.3. Role of the passive margin length for magma-poor and magma-rich passive margin settings

We investigated the influence of margin length and associated taper angle and rheology for endmember situations of short (50 km) and long (400 km) magma rich and magma poor passive margins (Fig. 8). Overall, these models of magma-poor and magma-rich passive margins are consistent with results derived from the reference models with a granulitic and doleritic crust, respectively (Fig. 5). In the situation of a magma-poor margin, a decrease of a narrow passive margin favours subduction at the margin (Fig. 8a) similarly to the model with average (150 km) margin length (Fig. 6). In contrast, an increase in margin length does not allow strain localization at the passive margin, but at the OCT, where serpentinites act as a weak zone (Fig. 8b). In the situation of a magma-rich margin, the shortening always creates intra-oceanic subduction initiation, regardless of margin length (Fig. 8 c-d), because the mafic intrusions and underplating lead to crust-mantle coupling as well as the strengthening of the margin (Fig. 7).

4. Discussion

4.1. Comparison to previous models

Although subduction zones often initiate through the lateral propagation from pre-existing subduction or polarity reversals (Crameri et al., 2020), other mechanisms that allow for the formation of new subduction plate boundaries must exist (Cloetingh et al., 2021; Crameri et al., 2020; Hall, 2019; McCarthy et al., 2018), most likely driven by far-field tectonic forcing (Gurnis et al., 2004), mantle suction flow (Baes & Sobolev, 2017), or a plume activity (van Hinsbergen et al., 2021). In that situation, the probability of subduction initiation increases in the vicinity of continental margins (e.g. Ulvrova et al., 2019). Previous modelling studies have shown that the ability of a passive margin to convert into a subduction zone is largely governed by the age and compositional differences in the mantle lithosphere across the ocean-continent transition (e.g., Auzemery et al., 2021a; Baes and Sobolev, 2017; Faccenna et al., 1999; Gurnis et al., 2004;

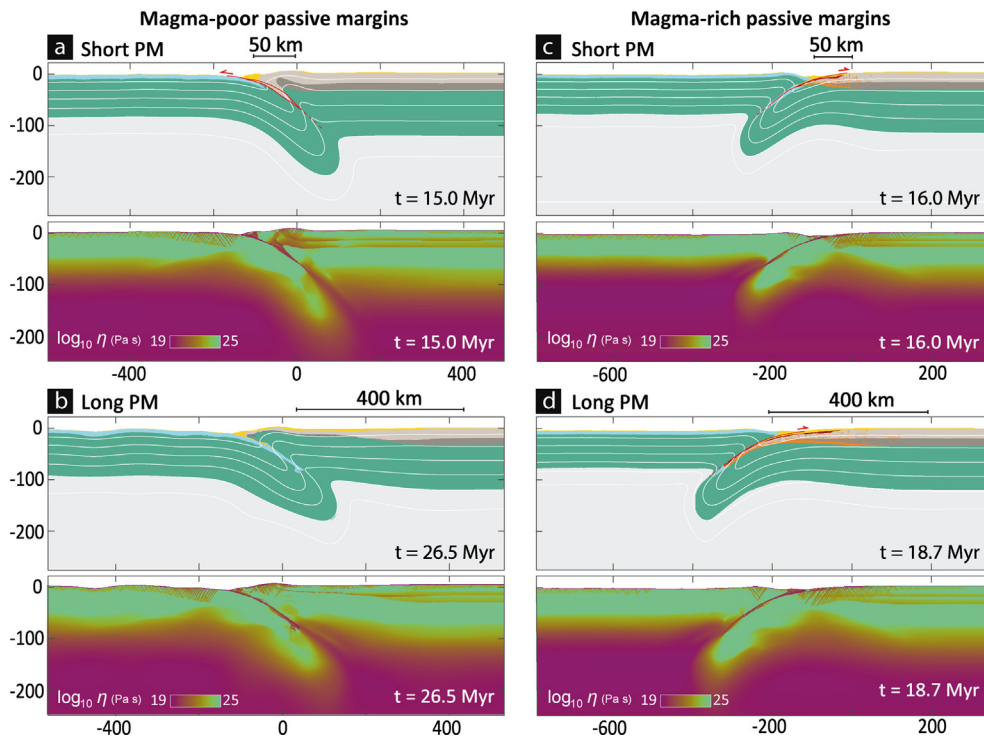


Fig. 8. Effect of passive margin length for magma-poor and magma-rich passive margin settings: mode of subduction initiation in case of shortening of (a) a 50 km magma-poor passive margin, (b) a 400 km long magma-poor passive margin, (c) a 50 km long magma-rich passive margin, (d) a 400 km long magma-rich passive margin. The bottom panel shows the viscosity for each model. Colour coding is the same as in Fig. 6&7. PM is passive margin. Model evolutions are available in the supplementary material S3.

Nikolaeva et al., 2011; Zhong and Li, 2019). Our models are in agreement with these general inferences, but further demonstrate that the degree of crust-mantle coupling has also a critical impact on the localisation of subduction zones (Fig. 3), which is further controlled by the geometry and the rheological layering of the continental crust at passive margins (Figs. 6 and 7). The latter controls where ductile flow dominates over plastic failure facilitating strain localization during the early phases of shortening. In our models this feature is inherent to the rheological stratification of the experiments, which is different to strain localization triggered by a thermal perturbation (Cramer & Kaus, 2010; Jaquet & Schmalholz, 2018; Thielmann & Kaus, 2012), although the deformational characteristics including the development of a major shear zone are similar in both cases. The degree of coupling at the passive margin can be governed by serpentinization of the lithospheric mantle (Fig. 6) or within the ductile continental crust. The linkage of a serpentinized shear zone with the ductile crust below proximal parts of the passive margin is key for the development of a large-scale shear zone that propagates into the mantle lithosphere to form the subduction plate boundary. Furthermore, we argue that serpentinized mantle lithosphere at MPPM is critical for initiating deformation at low stress levels. Kiss et al. (2020) obtained low stress levels for Moho temperatures between 525 and 600 °C at the onset of contraction. Our results further show that by explicit implementation of flow laws simulating weak serpentine rheologies, subduction initiation is mechanically feasible for Moho temperatures as low as ~460 °C. As such our results are in line with the study of Candiotti et al. (2020) who emphasises the importance of mechanical and geometrical heterogeneities at the onset of shortening for reducing the force needed for subduction initiation. It has been shown that the favourable age of oceanic lithosphere to develop a subduction zone at the margin is in the range of 50–110 Myr (e.g. Auzemery et al., 2020). Within this age window, density and strength contrasts across the margin coupled

to strain localization mechanisms provide suitable mechanical conditions for subduction initiation. However, a strong crust-mantle coupling of the continental lithosphere would prevent strain localization at the ocean-continent transition and generate a shift of deformation toward the oceanic domain (Fig. 7). Therefore, we agree that intra-oceanic subduction is more favourable in young oceanic basins (Auzemery et al., 2020; Faccenna et al., 1999; Zhong & Li, 2019), but it can also happen in old oceanic lithospheres for cases where the strength of the passive margin lithosphere is higher (e.g., through magmatism) compared to the oceanic lithosphere.

Together with the thickness of the ductile lower crust, the margin length is an important factor that influences strain localization through the crust and the mantle lithosphere. Therefore, for long (more than 300 km), decoupled and low angle passive margin, deformation is transmitted toward the continental crust (Fig. 4b) or the oceanic lithosphere (Fig. 4c). In the latter scenario, subduction is expected to occur at a strength minima which coincides with the presence of serpentine (Fig. 8b). Even if our concept of continental underthrusting is rarely mentioned in studies discussing plate tectonics, similar models have been obtained through reconstructions of the north African margin (Roure et al., 2012) and Cantabrian margin (Teixell et al., 2018; Viejo & Gallastegui, 2005) or in numerical studies (Kiss et al., 2020; Hamai et al., 2018).

4.2. Application to observations and reconstructions of subduction initiation near the former Adriatic passive continental margins

The evolution of continental passive margins along the former Adriatic micro-continent provides a unique opportunity to study subduction initiation in the vicinity of two continental rifted margin end-members. A MPPM and a MRPM developed over a similar pre-rifting continental structure and composition, with a similar oceanic lithospheric age at the time of subduction initiation and

with comparable convergence rates. The complexity of the Mediterranean system in terms of evolution and definition of units has resulted in numerous ideas of tectonic evolution and reconstructions (Capitanio & Goes, 2006; Csontos & Vörös, 2004; Handy et al., 2010; van Hinsbergen et al., 2020; Le Breton et al., 2020; Schmid et al., 2020; Stampfli & Hochard, 2009). Our analysis of tectonic evolution (Fig. 9) considers the quantitative reconstruction of van Hinsbergen et al. (2020) which is based on a recently updated quantitative definition of tectonic units and their lateral correlation in the critical area of Central and SE Europe (Schmid et al., 2020).

4.2.1. Subduction initiation along the former Adriatic MPPM presently exposed in the Alps

The onset of convergence in the Neotethys Ocean was roughly coeval with the onset of Middle Jurassic opening of the Piedmont-Liguria branch of the Alpine Tethys Ocean at ~170–160 Ma (Fig. 9a–c, Liati et al., 2005; Schaltegger et al., 2015). Rifting magmatism is minor or non-existent in the Alpine chain, with the exception of the eastern Southern Alps transitional area, where a Triassic phase of extension is associated with magmatism (e.g. Lustrino et al., 2019). A MPPM has been defined across several Alpine transects (Manatschal & Bernoulli, 1999; Manatschal & Müntener, 2009; Mohn et al., 2012; Müntener et al., 2004). After 60–70 Myr of slow oceanic seafloor spreading (McCarthy et al., 2020), the closure of the Piemont-Liguria branch of the Alpine Tethys ocean was initiated by subduction at the Adriatic passive margin (Fig. 10a, Manzotti et al., 2014; Marroni et al., 2017) and was driven by the northward motion of the Adriatic plate at a convergence rate of 0.9 to 1.5 cm.yr⁻¹ (Handy et al., 2010; van Hinsbergen et al., 2020). The Alpine Tethys Ocean was closed by the Eocene onset of continental collision, followed by the subse-

quent indentation of the Adriatic micro-continent in the Alps (e.g., Schmid et al., 2004a).

Our numerical modelling of MPPM (Fig. 6) displays striking similarities with reconstruction proposed for the Sesia-Dent Blanche transect (Fig. 10a). The Adriatic passive continental margin preserved a necking domain that recorded the formation of detachments in the upper-middle crust (Mohn et al., 2012; Manzotti et al., 2014). These detachments accommodated the extreme thinning of the Adria margin and created the large tectonic omission observed between the lower continental crust and exhumation of subcontinental mantle (Manatschal & Müntener, 2009; Müntener et al., 2004). The margin had a reconstructed width of 150–250 km at the time of subduction initiation (e.g. Beltrando et al., 2010), which was controlled by the presence of shear zones in the serpentinized exhumed mantle (Beltrando et al., 2010; Malatesta et al., 2011). The subsequent nappe emplacement was associated with high pressure-low temperature (HP-LT) metamorphism (Manzotti et al., 2014 and references therein) and the development of an accretionary wedge consisting of oceanic, continental, and subcontinental mantle material (Marroni et al., 2017). Moreover, the record of high pressure rocks in the Sesia unit, reaching eclogite facies conditions (e.g. Regis et al., 2014), suggest subduction of part of the passive continental margin. More specifically, higher pressure conditions recorded in the former proximal part of the passive margin (Manzotti et al., 2014) indicates that underthrusting started in the middle of the margin, probably close to the necking zone (Fig. 6a) at ~90–95 Ma. The basal units of the Sesia–Dent Blanche nappes were also affected by intense ductile shearing associated with pre-Alpine deformation (Beltrando et al., 2010). Observations from the Alps are in agreement with our modelling scenario where the initiation of subduction is driven by a basal thrust at the base of the continental

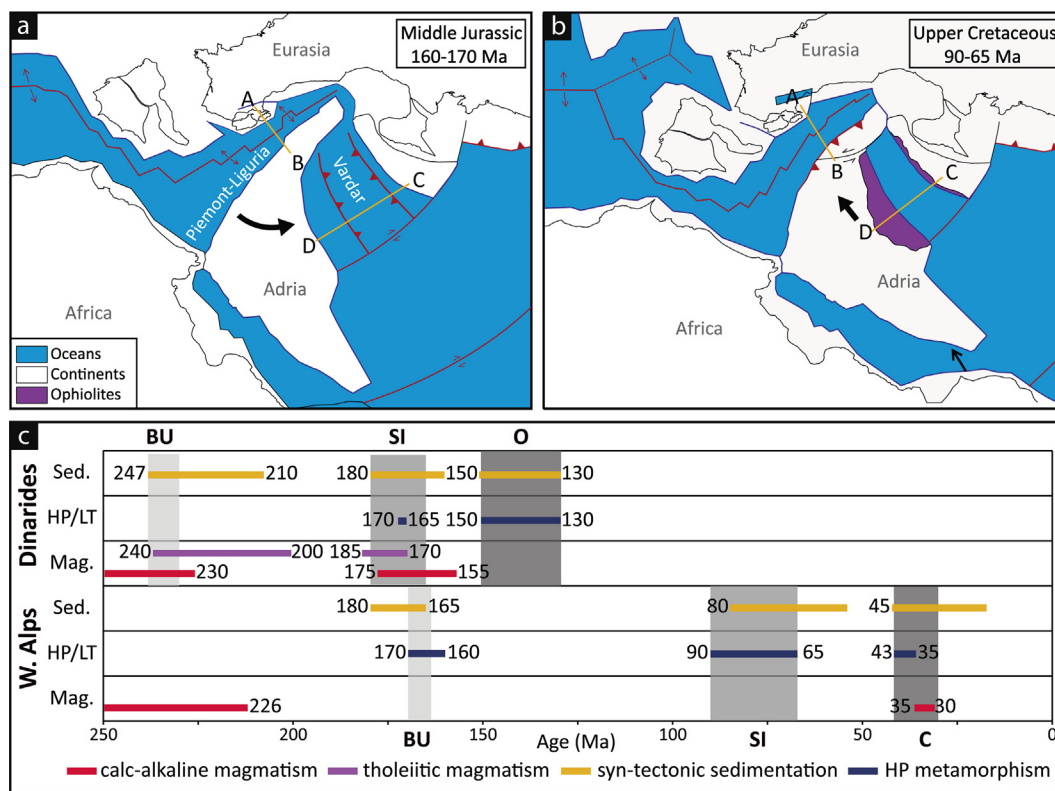


Fig. 9. Paleogeographic reconstructions of the western Neotethys domain, (compiled and adapted from Capitanio & Goes, 2006, van Hinsbergen et al., 2020, see also Table 4 in the supplementary material S4) (a) Middle Jurassic (170–160 Ma) (b) Upper Cretaceous (90–65 Ma). Black arrows indicate the relative motion of Adria. (c) Main tectono-magmatic and metamorphic events for oceanic basins in the Western Alps and the Dinarides relevant for subduction-initiation. B–U, SI, O and C denote break-up, subduction initiation, obduction and collision, respectively. A–B, C–D are the location of the profiles shown in Fig. 10.

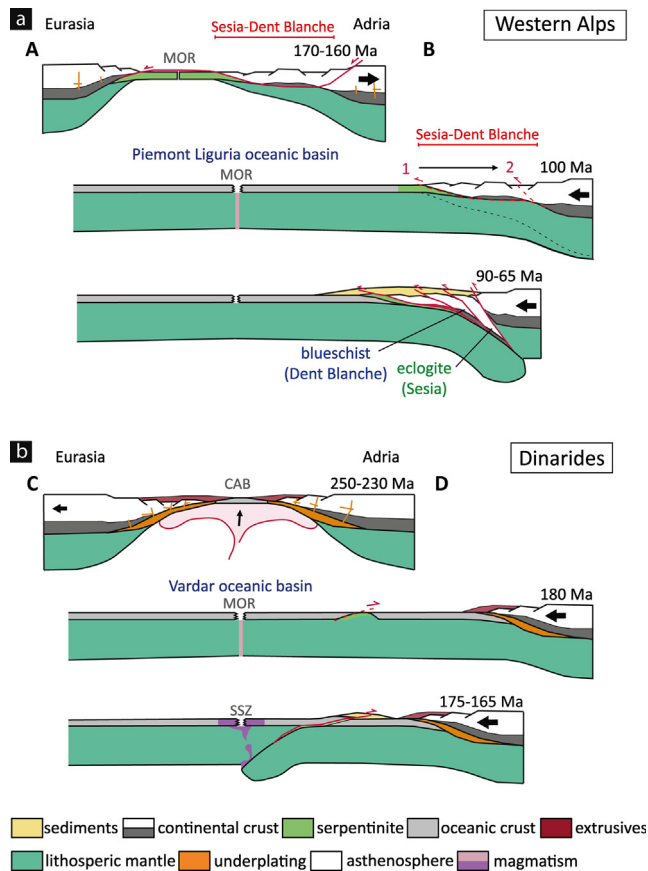


Fig. 10. Reconstruction of subduction initiation for the Alps and the Dinarides – Hellenides (adapted and simplified from Manzotti et al., 2014; Schmid et al., 2004b, 2008). (a) Shortening initiate subduction at the Alpine Tethys Adriatic MPPM. Development of shear zones in the serpentinitized exhumed mantle leads to nappe emplacement at the Adria continental margin. This evolution can be compared with our model of MPPM (Fig. 6b). (b) Development of intra-oceanic subduction in the vicinity of the Neotethys Adriatic MPPM. Locations AB, CD, of the cross-section are indicated in Fig. 9a and 9b. Black arrows indicate direction of extension and shortening respectively. CAB, MOR, SZZ stand for calc-alkaline basalt, mid-oceanic ridge and supra-subduction zone (magmatism).

crust along the passive margin, subsequently crosscut and duplicated in the overall nappe system (Fig. 6). The original reactivation of the serpentinitized mantle during contraction enabled the propagation of deformation toward the necking zone. Therefore, our study agrees that the necking domain localises subduction initiation, as previously inferred (Mohn et al., 2012), where the ductile lower crust is sufficiently thick to accommodate shortening (Fig. 6b). Our modelling also infers that the Sesia-Dent Blanche, Adriatic-derived extensional allochthon is not required to explain subduction initiation at the former Alpine passive margin (Manzotti et al., 2014).

4.2.2. Subduction initiation along the former Adriatic MRPM presently exposed in the Dinarides-Hellenides

Numerous studies have analysed the definition of tectonic units and their quantitative reconstruction in the Dinarides-Hellenides system of Central and SE Europe (e.g., Csontos & Vörös, 2004; Stampfli & Hochard, 2009). The most recent quantitative review (Schmid et al., 2020) and reconstruction (van Hinsbergen et al., 2020) account for a separation between the European and Adriatic continent by the onset of the opening of the northern branch of the Neotethys (or Vardar) Ocean at ~250–245 Ma (Fig. 9b–c, e.g., Schmid et al., 2020). These times are when large volumes of Middle – Late Triassic intrusive and extrusive magmatism were documented along the Adriatic continental margin, from the Hellenides

(e.g., Pe-Piper, 1998; Tsikouras et al., 2008) to the Dinarides (e.g., Pamic, 1984; Trubelja et al., 2004) and the eastern Southern Alps transitional area to the Alpine Tethys margin (e.g., De Min et al., 2020; Schmid et al., 2004a). The abundance of this basic to intermediate magmatism sourced from deep crustal or mantle levels (e.g., De Min et al., 2020; Pamic, 1984), associated with normal faulting and syn-kinematic deposition (e.g., Crisci et al., 1984; Robertson et al., 2009) infers partial melting during mantle upwelling and active rifting (e.g., Beltrán-Triviño et al., 2016). These observations combined with the Middle-Late Triassic age of calc-alkaline intermediate and mafic volcanism found in thrust ophiolitic mélanges (e.g. Pamic, 1984) testify the high magmatic budget along the Adriatic continental passive margin of the Dinarides-Hellenides (Fig. 10b). The subsequent closure of the northern Neotethys ocean by intra-oceanic subduction started during the late Early to Middle Jurassic, parallel to the ridge (Fig. 9a, ~160–180 Ma), inferred from dating metamorphic soles and mid-oceanic ridge (MOR) ophiolites, from occurrences of Late Triassic to Early Jurassic slices of scraped cherts and MOR basalts in thrust ophiolitic mélanges and from the Middle-Late Jurassic age of the obducted ophiolitic sheet (Bortolotti et al., 2013; Mikes et al., 2008; Maffione et al., 2015; Ustaszewski et al., 2009). Similar to the Adriatic continental rifted margin facing the Alpine Tethys, spreading in the Neotethys ocean lasted for 50–70 Myr until subduction initiation (e.g. Schmid et al., 2004b, van Hinsbergen et al., 2020, Fig. 9).

Plate reconstruction and paleo-magnetic studies suggest a convergence rate in the Neotethys Ocean of $1.5\text{--}2\text{ cm}\cdot\text{yr}^{-1}$ during 20 Myr (Capitanio & Goes, 2006; Handy et al., 2010; Le Breton et al., 2020 van Hinsbergen et al., 2020). This ocean was ultimately closed by the onset of the latest Cretaceous continental collision and the formation of the Sava suture zone between Adriatic- and European-derived continental units (e.g., Pamic, 1984; Schmid et al., 2020).

The comparison with our modelling study infers that the high magmatic budget of the Neotethys Adriatic continental rifted margin favoured the intra-oceanic subduction (Fig. 7). This mode of subduction initiation is driven by the strong rheological coupling of the passive margin, inhibiting the continent-ward propagation of deformation (Fig. 7). The subduction initiation took place during 10–15 Myr (Bortolotti et al., 2013), which is in agreement with our modelling results (Fig. 3b). The age of oceanic relics found in ophiolitic mélanges, combined with the age of obducted ophiolites, indicates that subduction initiated within the Early Jurassic part of the oceanic plate, although the occurrence of mid-ocean ridge ophiolites in contact with supra subduction zone ophiolites of the same age may also point to a subduction initiation close to the mid-oceanic ridge (Maffione et al., 2015). Although our models do not include a mid-oceanic ridge (See Auzemery et al., 2021b), they show that most shortening is initially localized in the place where the strength contrast is highest, i.e., at the ocean-continent transition, but migrates subsequently towards the oceanic domain, where the subduction zone forms at distances of less than 400 km from the margin (Fig. 5d).

Furthermore, our modelling predictions are comparable with previous observations in many other orogens containing ophiolitic belts, such as Anatolia (van Hinsbergen et al., 2016), Oman (Rioux et al., 2016; Saddiqi et al., 2006) or New-Caledonia (Lagabriele et al., 2013). These observations have shown that the short time span (<10 Myr) between supra-subduction spreading centres and ophiolites emplacement points towards intra-oceanic subduction initiation close to the margin. These observations are also in agreement with our inferences showing that a coupled margin deforms significantly less at the ocean-continent transition and a subduction zone develops further into the ocean. We also acknowledge the potential role of plate re-organization and oblique convergence

(Crameri et al., 2020; van Hinsbergen et al., 2020), or mantle rejuvenation by plume activity (Rolland et al., 2009), processes which are not accounted in our study.

5. Conclusions

Our thermo-mechanical models show that magma-poor passive margins with hyper-extended crust and exhumed serpentized mantle lithosphere are favourable sites for induced subduction initiation. The serpentized mantle facilitates strain localization and progressive development of a major shear zone that ultimately links up with zone of high strain that developed within the ductile lower continental crust in the necking zone. Shearing then propagates into the mantle lithosphere to initiate a subduction plate boundary. In contrast, passive margins intruded and underplated by magmatism favour intra-oceanic subduction initiation. These margins are rheologically coupled and stronger, which induces distributed deformation during the early shortening, while the subsequent deformation migrates within the oceanic lithosphere. These results indicate that the rheological and geometrical configuration of the passive margin, inherited from the magmatic budget during continental rifting phase, is critical for strain localisation mechanisms during the early stages of deformation and shows that subduction initiation is mechanically feasible for Moho temperatures below 500 °C.

Our modelling results can be applied to the unique case of subduction initiation along two contrasting types of margins associated with the same Adriatic continental microplate. These results provide a mechanical explanation for subduction initiation at the ocean-continent transition in the western Alps and within the Neotethys ocean in the Dinarides-Hellenides orogenic systems, representing end-members of subduction initiation at magma-poor and magma-rich margins, respectively.

CRedit authorship contribution statement

A. Auzemery: Conceptualization, Investigation, Formal analysis, Validation, Writing – original draft. **P. Yamato:** Software, Validation, Writing – review & editing. **T. Duretz:** Software, Conceptualization, Methodology, Writing – review & editing. **E. Willingshofer:** Funding acquisition, Supervision, Writing – review & editing. **L. Matenco:** Validation, Writing – review & editing. **K. Porkoláb:** Conceptualization, Visualization, Writing – review & editing.

Declaration of Competing Interest

The authors declare that they have no known competing financial interests or personal relationships that could have appeared to influence the work reported in this paper.

Acknowledgement, Samples, and Data

The research project was funded by the European Union's EU Framework Programme for Research and Innovation Horizon 2020 "Subitop" under Grant Agreement No 674899. We are indebted to the editor and the reviewers for their valuable comments and suggestions, which have significantly improved the original manuscript.

Code availability

Researchers interested in using the numerical code should contact the authors. The code is available from the authors upon reasonable request.

Appendix A. Supplementary material

Supplementary data to this article can be found online at <https://doi.org/10.1016/j.gr.2021.11.012>.

References

- Arcay, D., Lallemand, S., Abecassis, S., Garel, F., 2020. Can subduction initiation at a transform fault be spontaneous? *Solid Earth* 11 (1), 37–62.
- Artemieva, I.M., 2009. The continental lithosphere: reconciling thermal, seismic, and petrologic data. *Lithos* 109 (1–2), 23–46.
- Auzemery, Antoine, Willingshofer, Ernst, Sokoutis, Dimitrios, Brun, Jean-Pierre, Cloetingh, Sierd A.P.L., 2021a. Passive margin inversion controlled by stability of the mantle lithosphere. *Tectonophysics* 817 (229042). <https://doi.org/10.24416/UU01-CMK25L>. <https://doi.org/10.1016/j.tecto.2021.229042>.
- Auzemery, Antoine, Willingshofer, Ernst, Yamato, Philippe, Duretz, Thibault, Beekman, Fred, 2021b. Kinematic boundary conditions favouring subduction initiation at passive margins over subduction at mid-oceanic ridges. In: *Front. Earth Sci.* 9 (1131), 765893. <https://doi.org/10.3389/feart.2021.765893> <https://www.frontiersin.org/article/10.3389/feart.2021.765893>.
- Auzemery, A., Willingshofer, E., Yamato, P., Duretz, T., Sokoutis, D., 2020. Strain localization mechanisms for subduction initiation at passive margins. *GPC*. <https://doi.org/10.1016/j.gloplacha.2020.103323>.
- Baer, M., Sobolev, S.V., 2017. Mantle flow as a trigger for subduction initiation: A missing element of the Wilson Cycle concept. *GGG* 18 (12), 4469–4486.
- Bayrakci, G., Minshull, T., Sawyer, D., Reston, T.J., Klaeschen, D., Papenberg, C., Ranero, C., Bull, J., Davy, R., Shillington, D., 2016. Fault-controlled hydration of the upper mantle during continental rifting. *Nat. Geosci.* 9 (5), 384.
- Beaussier, S.J., Gerya, T.V., Burg, J.-P., 2019. Near-ridge initiation of intraoceanic subduction: Effects of inheritance in 3D numerical models of the Wilson Cycle. *Tectonophysics* 763, 1–13.
- Beltrán-Triviño, A., Winkler, W., von Quadt, A., Gálhofer, D., 2016. Triassic magmatism on the transition from Variscan to Alpine cycles: evidence from U-Pb, Hf, and geochemistry of detrital minerals. *Swiss J. Geosci.* 109 (3), 309–328.
- Beltrando, M., Rubatto, D., Manatschal, G., 2010. From passive margins to orogens: The link between ocean-continent transition zones and (ultra) high-pressure metamorphism. *Geology* 38 (6), 559–562.
- Bercović, D., Mulyukova, E., 2021. Evolution and demise of passive margins through grain mixing and damage. *Proc. Nation. Acad. Sci.* 118 (4).
- Bortolotti, V., Chiari, M., Marroni, M., Pandolfi, L., Principi, G., Saccani, E., 2013. Geodynamic evolution of ophiolites from Albania and Greece (Dinaric-Hellenic belt): one, two, or more oceanic basins? *IJEAS* 102 (3), 783–811.
- Brun, J., Beslier, M., 1996. Mantle exhumation at passive margins. *Earth Planet. Sci. Lett.* 142 (1–2), 161–173.
- Burov, E.B., 2011. Rheology and strength of the lithosphere. *Mar. Pet. Geol.* 28 (8), 1402–1443.
- Candiotti, L.G., Schmalholz, S.M., Duretz, T., 2020. Impact of upper mantle convection on lithosphere hyperextension and subsequent horizontally forced subduction initiation. *Solid Earth* 11 (6), 2327–2357.
- Capitanio, F.A., Goes, S., 2006. Mesozoic spreading kinematics: consequences for Cenozoic Central and Western Mediterranean subduction. *Geol.* 165 (3), 804–816.
- Clerc, C., Ringenbach, J.-C., Jolivet, L., Ballard, J.-F., 2018. Rifted margins: Ductile deformation, boudinage, continentward-dipping normal faults and the role of the weak lower crust. *Gondwana Res.* 53, 20–40.
- Cloetingh, S., Koptev, A., Kovács, I., Gerya, T., Beniest, A., Willingshofer, E., Ehlers, T. A., Andrić-Tomašević, N., Botsyun, S., Eizenhöfer, P.R., 2021. Plume-Induced Sinking of Intracontinental Lithospheric Mantle: An Overlooked Mechanism of Subduction Initiation? *GGG* 22 (2), e2020GC009482.
- Cloetingh, S., Wortel, M., Vlaar, N., 1984. Passive margin evolution, initiation of subduction and the Wilson cycle. In: Zwart, H., Behr, H., Je, O. (Eds.), *Tectonophysics*, vol. 109, pp. 147–163.
- Cloetingh, S., Wortel, R., Vlaar, N., 1989. On the initiation of subduction zones. In: *Subduction Zones Part II*. Birkhäuser Verlag, pp. 7–25.
- Corti, G., 2009. Continental rift evolution: from rift initiation to incipient break-up in the Main Ethiopian Rift, East Africa. *Earth-Sci. Rev.* 96 (1–2), 1–53.
- Crameri, F., Kaus, B.J., 2010. Parameters that control lithospheric-scale thermal localization on terrestrial planets. *Geophys. Res. Lett.* 37 (9).
- Crameri, F., Magni, V., Domeier, M., Shephard, G.E., Chotalia, K., Cooper, G., Eakin, C. M., Grima, A.G., Güler, D., Király, Á., 2020. A transdisciplinary and community-driven database to unravel subduction zone initiation. *Nat. Commun.* 11 (1), 1–14.
- Crisi, C., Ferrara, G., Mazzuoli, R., Rossi, P., 1984. Geochemical and geochronological data on Triassic volcanism of the Southern Alps of Lombardy (Italy): genetic implications. *Geol. Rundsch.* 73 (1), 279–292.
- Csontos, L., Vörös, A., 2004. Mesozoic plate tectonic reconstruction of the Carpathian region. *Palaeogeogr., Palaeoclimatol., Palaeoecol.* 210 (1), 1–56.
- De Min, A., Velicogna, M., Ziberna, L., Chiaradia, M., Alberti, A., Marzoli, A., 2020. Triassic magmatism in the European Southern Alps as an early phase of Pangea break-up. *GeoM*, 1–23.
- Duarte, J.C., Rosas, F.M., Terrinha, P., Schellart, W.P., Boutelier, D., Gutscher, M.-A., Ribeiro, A., 2013. Are subduction zones invading the Atlantic? Evidence from the southwest Iberia margin. *Geology* 41 (8), 839–842.

- Duretz, T., Petri, B., Mohn, G., Schmalholz, S., Schenker, F., Müntener, O., 2016. The importance of structural softening for the evolution and architecture of passive margins. *Sci. Rep.* 6 (1), 1–7.
- Dymkova, D., Gerya, T., 2013. Porous fluid flow enables oceanic subduction initiation on Earth. *Geophys. Res. Lett.* 40 (21), 5671–5676.
- Faccenna, C., Giardini, D., Davy, P., Argentieri, A., 1999. Initiation of subduction at Atlantic-type margins: Insights from laboratory experiments. *JGRB: Solid Earth* 104 (B2), 2749–2766.
- Geoffroy, L., 2005. Volcanic passive margins. *C.R. Geosci.* 337 (16), 1395–1408.
- Gerya, T.V., Stern, R.J., Baes, M., Sobolev, S.V., Whattam, S.A., 2015. Plate tectonics on the Earth triggered by plume-induced subduction initiation. *Nat.* 527 (7577), 221–225.
- Goren, L., Aharonov, E., Mulugeta, G., Koyi, H.A., Mart, Y., 2008. Ductile deformation of passive margins: A new mechanism for subduction initiation. *JGRB: Solid Earth* 113 (B8). <https://doi.org/10.1029/2005JB004179>.
- Guillot, S., Schwartz, S., Reynard, B., Agard, P., Prigent, C., 2015. Tectonic significance of serpentinites. *Tectonophysics* 646, 1–19.
- Gülcher, A., Beaussier, S., Gerya, T., 2019. On the formation of oceanic detachment faults and their influence on intra-oceanic subduction initiation: 3D thermomechanical modeling. *Earth Planet. Sci. Lett.* 506, 195–208.
- Gurnis, M., Hall, C., Lavier, L., 2004. Evolving force balance during incipient subduction. *GGG* 5 (7).
- Hall, R., 2019. The subduction initiation stage of the Wilson cycle. *J. Geol. Soc. London* 470 (1), 415–437.
- Hamai, L., Petit, C., Le Pourhiet, L., Yelles-Chaouche, A., Déverchère, J., Beslier, M.-O., Abtout, A., 2018. Towards subduction inception along the inverted North African margin of Algeria? Insights from thermo-mechanical models. *Earth Planet. Sci. Lett.* 501, 13–23.
- Handy, M.R., Schmid, S.M., Bousquet, R., Kissling, E., Bernoulli, D., 2010. Reconciling plate-tectonic reconstructions of Alpine Tethys with the geological-geophysical record of spreading and subduction in the Alps. *Earth-Sci. Rev.* 102 (3–4), 121–158.
- Hansen, F., Carter, N., 1983. Semibrittle creep of dry and wet Westerly granite at 1000 MPa. Paper presented at the The 24th US Symposium on Rock Mechanics (USRMS).
- Hilairet, N., Reynard, B., Wang, Y., Daniel, I., Merkel, S., Nishiyama, N., Petitgirard, S., 2007. High-pressure creep of serpentine, interseismic deformation, and initiation of subduction. *Science* 318 (5858), 1910–1913.
- Hirth, G., Kohlstedt, D., 2003. Rheology of the upper mantle and the mantle wedge: A view from the experimentalists. *Geophys. Monogr.-Am. Geophys. Union* 138, 83–106.
- Houseman, G.A., McKenzie, D.P., Molnar, P., 1981. Convective instability of a thickened boundary layer and its relevance for the thermal evolution of continental convergent belts. *JGRB: Solid Earth* 86 (B7), 6115–6132.
- Jaquet, Y., Schmalholz, S.M., 2018. Spontaneous ductile crustal shear zone formation by thermal softening and related stress, temperature and strain rate evolution. *Tectonophysics* 746, 384–397.
- Kelemen, P.B., Holbrook, W.S., 1995. Origin of thick, high-velocity igneous crust along the US East Coast Margin. *JGRB: Solid Earth* 100 (B6), 10077–10094.
- Kiss, D., Candioti, L.G., Duretz, T., Schmalholz, S.M., 2020. Thermal softening induced subduction initiation at a passive margin. *Geofl.* 220 (3), 2068–2073.
- Koptev, A., Beniest, A., Gerya, T., Ehlers, T.A., Jolivet, L., Leroy, S., 2019. Plume-induced breakup of a subducting plate: Microcontinent formation without cessation of the subduction process. *Geophys. Res. Lett.* 46 (7), 3663–3675.
- Koptev, A., Cloetingh, S., Ehlers, T.A., 2021. Longevity of small-scale (“baby”) plumes and their role in lithospheric break-up. *Geofl.*
- Kronenberg, A.K., Kirby, S.H., Pinkston, J., 1990. Basal slip and mechanical anisotropy of biotite. *JGRB: Solid Earth* 95 (B12), 19257–19278.
- Lagabriele, Y., Chauvet, A., Ulrich, M., Guillot, S., 2013. Passive obduction and gravity-driven emplacement of large ophiolite sheets: The New Caledonia ophiolite (SW Pacific) as a case study? *Bull. Soc. Geol. Fr.* 184 (6), 545–556.
- Le Breton, E., Brune, S., Ustaszewski, K., Zahirovic, S., Seton, M., Müller, R.D., 2020. Kinematics and extent of the Piemont-Liguria Basin—implications for subduction processes in the Alps. *Solid Earth Discuss.*, 1–42.
- Li, J., Hu, X., Garzanti, E., Banerjee, S., BouDagher-Fadel, M., 2020. Late Cretaceous topographic doming caused by initial upwelling of Deccan magmas: Stratigraphic and sedimentological evidence. *GSA Bulletin* 2019 132 (3–4), 835–849.
- Liati, A., Froitzheim, N., Fanning, C.M., 2005. Jurassic ophiolites within the Valais domain of the Western and Central Alps: geochronological evidence for re-irrigation of oceanic crust. *Contrib. Miner. Petrol.* 149 (4), 446–461.
- Lustrino, M., Abbas, H., Agostini, S., Gaggiati, M., Carminati, E., Gianolla, P., 2019. Origin of Triassic magmatism of the Southern Alps (Italy): Constraints from geochemistry and Sr-Nd-Pb isotopic ratios. *Gondwana Res.* 75, 218–238.
- Mackwell, S., Zimmerman, M., Kohlstedt, D., 1998. High-temperature deformation of dry diabase with application to tectonics on Venus. *JGRB: Solid Earth* 103 (B1), 975–984.
- Maffione, M., Thieulot, C., Van Hinsbergen, D.J., Morris, A., Plümpner, O., Spakman, W., 2015. Dynamics of intraoceanic subduction initiation: 1. Oceanic detachment fault inversion and the formation of supra-subduction zone ophiolites. *GGG* 16 (6), 1753–1770.
- Malatesta, C., Gerya, T., Scambelluri, M., Federico, L., Crispini, L., Capponi, G., 2011. Serpentine channel and the role of serpentinite buoyancy for exhumation of HP rocks (Voltri Massif, Western Alps). Paper presented at the Goldschmidt conference abstracts.
- Manatschal, G., Bernoulli, D., 1999. Architecture and tectonic evolution of nonvolcanic margins: Present-day Galicia and ancient Adria. *Tectonics* 18 (6), 1099–1119.
- Manatschal, G., Froitzheim, N., Rubenach, M., Turrin, B., 2001. The role of detachment faulting in the formation of an ocean-continent transition: insights from the Iberia Abyssal Plain. *J. Geol. Soc. London, Special Publications* 187 (1), 405–428.
- Manatschal, G., Müntener, O., 2009. A type sequence across an ancient magma-poor ocean-continent transition: the example of the western Alpine Tethys ophiolites. *Tectonophysics* 473 (1–2), 4–19.
- Manzotti, P., Ballevre, M., Zucali, M., Robyr, M., Engi, M., 2014. The tectonometamorphic evolution of the Sesia-Dent Blanche nappes (internal Western Alps): review and synthesis. *Swiss J. Geosci.* 107 (2–3), 309–336.
- Marroni, M., Meneghini, F., Pandolfi, L., 2017. A revised subduction inception model to explain the Late Cretaceous, double-vergent orogen in the precollisional western Tethys: Evidence from the Northern Apennines. *Tectonics* 36 (10), 2227–2249.
- McCarthy, A., Chelle-Michou, C., Müntener, O., Arculus, R., Blundy, J., 2018. Subduction initiation without magmatism: The case of the missing Alpine magmatic arc. *Geology* 46 (12), 1059–1062.
- McCarthy, A., Tugend, J., Mohn, G., Candioti, L., Chelle-Michou, C., Arculus, R., Schmalholz, S.M., Müntener, O., 2020. A case of Ampferer-type subduction and consequences for the Alps and the Pyrenees. *Am. J. Sci.* 320 (4), 313–372.
- Mikes, T., Christ, D., Petri, R., Dunkl, I., Frei, D., Báldi-Beke, M., Reitner, J., Wemmer, K., Hrvatović, H., von Eynatten, H., 2008. Provenance of the bosnian Flysch. *Swiss J. Geosci.* 101 (1), 31–54.
- Mohn, G., Manatschal, G., Beltrando, M., Masini, E., Kuszniir, N., 2012. Necking of continental crust in magma-poor rifted margins: Evidence from the fossil Alpine Tethys margins. *Tectonics* 31 (1).
- Müntener, O., Pettke, T., Desmurs, L., Meier, M., Schaltegger, U., 2004. Refertilization of mantle peridotite in embryonic ocean basins: trace element and Nd isotopic evidence and implications for crust-mantle relationships. *Earth Planet. Sci. Lett.* 221 (1–4), 293–308.
- Nikolaeva, K., Gerya, T.V., Marques, F.O., 2010. Subduction initiation at passive margins: Numerical modeling. *JGRB: Solid Earth* 115 (B3). <https://doi.org/10.1029/2009JB006549>.
- Nikolaeva, K., Gerya, T.V., Marques, F.O., 2011. Numerical analysis of subduction initiation risk along the Atlantic American passive margins. *Geology* 39 (5), 463–466.
- Pamir, J.J., 1984. Triassic magmatism of the Dinarides in Yugoslavia. *Tectonophysics* 109 (3–4), 273–307.
- Parsons, B., McKenzie, D., 1978. Mantle convection and the thermal structure of the plates. *JGRB: Solid Earth* 83 (B9), 4485–4496.
- Paton, D., Pindell, J., McDermott, K., Bellingham, P., Horn, B., 2017. Evolution of seaward-dipping reflectors at the onset of oceanic crust formation at volcanic passive margins: Insights from the South Atlantic. *Geology* 45 (5), 439–442.
- Pe-Piper, G., 1998. The nature of Triassic extension-related magmatism in Greece: evidence from Nd and Pb isotope geochemistry. *GeoM* 135 (3), 331–348.
- Ranalli, G., 1995. Rheology of the Earth. Springer Science & Business Media.
- Regis, D., Rubatto, D., Darling, J., Cenki-Tok, B., Zucali, M., Engi, M., 2014. Multiple metamorphic stages within an eclogite-facies terrane (Sesia Zone, Western Alps) revealed by Th-U-Pb petrochronology. *JPet* 55 (7), 1429–1456.
- Reston, T., Manatschal, G., 2011. Rifted margins: Building blocks of later collision. In *Arc-continent collision*. Springer, pp. 3–21.
- Rioux, M., Garber, J., Bauer, A., Bowring, S., Searle, M., Kelemen, P., Hacker, B., 2016. Synchronous formation of the metamorphic sole and igneous crust of the Semai ophiolite: New constraints on the tectonic evolution during ophiolite formation from high-precision U-Pb zircon geochronology. *Earth Planet. Sci. Lett.* 451, 185–195.
- Robertson, A., Karamata, S., Šarić, K., 2009. Overview of ophiolites and related units in the Late Palaeozoic-Early Cenozoic magmatic and tectonic development of Tethys in the northern part of the Balkan region. *Lithos* 108 (1–4), 1–36.
- Rolland, Y., Galoyan, G., Bosch, D., Sosson, M., Corsini, M., Fornari, M., Verati, C., 2009. Jurassic back-arc and Cretaceous hot-spot series in the Armenian ophiolites—Implications for the obduction process. *Lithos* 112 (3–4), 163–187.
- Roure, F., Casero, P., Addoum, B., 2012. Alpine inversion of the North African margin and delamination of its continental lithosphere. *Tectonics* 31 (3). <https://doi.org/10.1029/2011TC002989>.
- Rybacki, E., Dresen, G., 2004. Deformation mechanism maps for feldspar rocks. *Tectonophysics* 382 (3–4), 173–187.
- Saddiqi, O., Michard, A., Goffe, B., Poupeau, G., Oberhänsli, R., 2006. Fission-track thermochronology of the Oman Mountains continental windows, and current problems of tectonic interpretation. *Bull. Soc. Geol. Fr.* 177 (3), 127–134.
- Sapin, F., Ringenbach, J.-C., Clerc, C., 2021. Rifted margins classification and forcing parameters. *Sci. Rep.* 11 (1), 1–17.
- Schaltegger, U., Ulianov, A., Müntener, O., Ovtcharova, M., Peytcheva, I., Vonlanthen, P., Vennemann, T., Antognini, M., Girlanda, F., 2015. Megacrystic zircon with planar fractures in miaskite-type nepheline pegmatites formed at high pressures in the lower crust (Ivrea Zone, southern Alps, Switzerland). *Am. Min.* 100 (1), 83–94.
- Schmid, S., Fügenschuh, B., Kissling, E., Schuster, R., 2004a. *Three lithospheric transects across the Alps and their forelands*. Paper presented at the Swiss Geoscience Meeting, Lausanne.
- Schmid, S.M., Fügenschuh, B., Kissling, E., Schuster, R., 2004b. Tectonic map and overall architecture of the Alpine orogen. *Eclogae Geol. Helv.* 97 (1), 93–117.

- Schmid, S.M., Fügenschuh, B., Kounov, A., Mačenco, L., Nievergelt, P., Oberhänsli, R., Pleuger, J., Schefer, S., Schuster, R., Tomljenović, B., 2020. Tectonic units of the Alpine collision zone between Eastern Alps and western Turkey. *Gondwana Res.* 78, 308–374.
- Sengör, A.C., Burke, K., 1978. Relative timing of rifting and volcanism on Earth and its tectonic implications. *Geophys. Res. Lett.* 5 (6), 419–421.
- Sobolev, S.V., Brown, M., 2019. Surface erosion events controlled the evolution of plate tectonics on Earth. *Nat.* 570 (7759), 52–57.
- Stampfli, G.M., Hochard, C., 2009. Plate tectonics of the Alpine realm. *J. Geol. Soc. London, Special Publications* 327 (1), 89–111.
- Stern, R.J., Gerya, T., 2018. Subduction initiation in nature and models: A review. *Tectonophysics* 746, 173–198.
- Teixell, A., Labaume, P., Ayarza, P., Espurt, N., de Saint Blanquat, M., Lagabriele, Y., 2018. Crustal structure and evolution of the Pyrenean-Cantabrian belt: A review and new interpretations from recent concepts and data. *Tectonophysics* 724, 146–170.
- Thielmann, M., Kaus, B.J., 2012. Shear heating induced lithospheric-scale localization: Does it result in subduction? *Earth Planet. Sci. Lett.* 359, 1–13.
- Trubelja, F., Burgath, K.-P., Marchig, V., 2004. Triassic magmatism in the area of the Central Dinarides (Bosnia and Herzegovina): geochemical resolving of tectonic setting. *Geologia Croatica* 57 (2), 159–170.
- Tsikouras, B., Pe-Piper, G., Piper, D.J., Hatzipanagiotou, K., 2008. Triassic rift-related komatiite, picrite and basalt, Pelagonian continental margin, Greece. *Lithos* 104 (1–4), 199–215.
- Tugend, J., Gillard, M., Manatschal, G., Nirrengarten, M., Harkin, C., Epin, M.-E., Sauter, D., Autin, J., Kuszniir, N., Mcdermott, K., 2020. Reappraisal of the magma-rich versus magma-poor rifted margin archetypes. *J. Geol. Soc. London, Special Publications* 476 (1), 23–47.
- Turcotte, D., Schubert, G., 2014. *Geodynamics*. Cambridge university press.
- Ulvrova, M.M., Coltice, N., Williams, S., Tackley, P.J., 2019. Where does subduction initiate and cease? A global scale perspective. *Earth Planet. Sci. Lett.* 528, 115836.
- Ustaszewski, K., Schmid, S.M., Lugović, B., Schuster, R., Schaltegger, U., Bernoulli, D., Hottinger, L., Kounov, A., Fügenschuh, B., Schefer, S., 2009. Late Cretaceous intra-oceanic magmatism in the internal Dinarides (northern Bosnia and Herzegovina): Implications for the collision of the Adriatic and European plates. *Lithos* 108 (1–4), 106–125.
- van de Lagemaat, S.H., Swart, M.L., Vaes, B., Kusters, M.E., Boschman, L.M., Burton-Johnson, A., Bijl, P.K., Spakman, W., van Hinsbergen, D.J., 2021. Subduction initiation in the Scotia Sea region and opening of the Drake Passage: When and why? *Earth-Sci. Rev.*, 103551.
- van Hinsbergen, D.J., Maffione, M., Plunder, A., Kaymakci, N., Ganerød, M., Hendriks, B.W., Corfu, F., Güler, D., de Gelder, G.I., Peters, K., 2016. Tectonic evolution and paleogeography of the Kırşehir Block and the Central Anatolian Ophiolites, Turkey. *Tectonics* 35 (4), 983–1014.
- van Hinsbergen, D.J., Steinberger, B., Guilmette, C., Maffione, M., Güler, D., Peters, K., Plunder, A., McPhee, P.J., Gaina, C., Advokaat, E.L., 2021. A record of plume-induced plate rotation triggering subduction initiation. *Nat. Geosci.* 14 (8), 626–630.
- van Hinsbergen, D.J., Torsvik, T.H., Schmid, S.M., Mačenco, L.C., Maffione, M., Vissers, R.L., Güler, D., Spakman, W., 2020. Orogenic architecture of the Mediterranean region and kinematic reconstruction of its tectonic evolution since the Triassic. *Gondwana Res.* 81, 79–229.
- Viejo, G.F., Gallastegui, J., 2005. The ESCI-N Project after a decade: a synthesis of the results and open questions. *Trabajos de geología* 25, 9–27.
- Whattam, S.A., Stern, R.J., 2015. Late Cretaceous plume-induced subduction initiation along the southern margin of the Caribbean and NW South America: The first documented example with implications for the onset of plate tectonics. *Gondwana Res.* 27 (1), 38–63.
- White, R.S., Spence, G.D., Fowler, S.R., McKenzie, D.P., Westbrook, G.K., Bowen, A.N., 1987. Magmatism at rifted continental margins. *Nat.* 330 (6147), 439–444.
- Yamato, P., Husson, L., Becker, T.W., Pedoja, K., 2013. Passive margins getting squeezed in the mantle convection vice. *Tectonics* 32 (6), 1559–1570. <https://doi.org/10.1002/2013TC003375>.
- Zhong, X., Li, Z.H., 2019. Forced Subduction Initiation at Passive Continental Margins: Velocity-Driven Versus Stress-Driven. *Geophys. Res. Lett.* 46 (20), 11054–11064.
- Zhou, X., Li, Z.-H., Gerya, T.V., Stern, R.J., 2020. Lateral propagation-induced subduction initiation at passive continental margins controlled by preexisting lithospheric weakness. *Sci. Adv.* 6 (10), eaaz1048.